AIAA JOURNAL
Vol. 36, No. 7, July 1998

Compressive Behavior of Multiply Delaminated Composite Laminates Part 1: Experiment and Analytical Development

Hiroshi Suemasu,* Tatsuya Kumagai,† and Katsuhisa Gozu‡
Sophia University, Tokyo 102, Japan

The basic mechanics and mechanism concerning compressive stability of composite laminates with multiple circular delaminations is studied analytically and experimentally. An experimental program, employing two types of quasi-isotropic laminates with a conventional and toughened epoxy resin, is used to evaluate the validity of the mechanistic model and further demonstrate the accuracy of finite element analysis conducted in the associated paper. Embedded delaminations are introduced at regular intervals in the thickness direction. The loading edges are fixed, and the side edges are simply supported. Although the buckling load does not depend on the matrix resin toughness, the strength is affected by the toughness. In the analysis, a buckling equation is derived using the Rayleigh–Ritz method, based on classical plate theory and solved as an eigenvalue problem. This method is chosen due to its efficiency. As the buckling mode of the lowest buckling load becomes physically admissible due to the assumptions of equally spaced delaminations and the classical plate theory, the contact problem does not need to be considered, that is, all of the delaminated portions deform by the same amount and do not overlap one another even without any constraints. The buckling loads analytically obtained agree well with experimental and finite element results described in the associated paper. The effects of size and number of circular delaminations on the buckling and failure load are also discussed in detail.

I. Introduction

SIGNIFICANT loss of compressive strength for composite laminates subjected to low-velocity impact of a foreign object, known as compression after impact (CAI), is an important issue in the design of composite structures, as the decreased compressive strength often becomes of critical concern.

Delamination beneath the impact point is thought to be the main reason for significant reductions in compressive strength for damaged plates, and the effect of a delamination or delaminations on buckling and postbuckling properties of composite plates has been studied analytically and experimentally by many researchers. In particular, one-dimensional-beam-type models of delaminated laminates have been investigated by many workers due to the simplicity of the modeling, e.g., Refs. 1–6. Although these studies have shown the possibility of significant decreases in compressive buckling and postbuckling properties, the model cannot explain the real CAI problem well, and so research on two-dimensional-plate-type modeling is thought necessary. Analytical and numerical work on the effect of delamination on compressive behavior for two-dimensional plates has been limited to special cases. For example, Chai and Babcock[7] and Yin and Jane[8] analytically studied compressive buckling behavior for surface elliptical delamination using the Rayleigh–Ritz method, whereas Whitcomb and Shivakumar[9] studied a similar problem numerically by the finite element method. Shahwan and Waas[10] considered the contact problem when the postbuckling behavior of surface delamination was investigated. Suemasu[11–13] and Suemasu et al.[14] also studied the buckling and postbuckling response of square plates with a through-width delamination using the Rayleigh–Ritz method and showed that coupling of the local and global deformation played a critical role in buckling and postbuckling behavior. Klug et al.[15] recently investigated the postbuckling response of a plate with an elliptical delamination using a finite element method and discussed the stability of the delamination crack using an energy release rate distribution.

Impact tests, e.g., Refs. 16–19, have shown that multiple delaminations, which are relatively small in size compared to the plate, were produced at the impact point in CF/epoxy plates, with the compressive strength being reduced to approximately one-third that of the virgin plates. The reduction in compressive strength following impact was attributed mainly to the existence of multiple delaminations. Thus, the effect of multiple delaminations on compressive behavior for composite plates should be further investigated.

Suemasu[20] previously has analytically studied the effect of multiple delaminations on the buckling behavior of rectangular plates. The present work is concerned with the multiple circular delaminations on compressive buckling and failure loads, which are studied experimentally in combination with an analysis based on the Rayleigh–Ritz method. Validity of the present analysis was also established through comparison with finite element results obtained in a companion paper.[21]

II. Experiment

A. Specimen and Test Setup

Plain-woven, fabric-reinforced, composite quasi-isotropic laminates (Toray T400 carbon/epoxy, 12 plies, $V_f \approx 50\%$, $[0, 90/\pm 45/0, 90/\pm 45/0, 90/\pm 45\ \text{deg}]_s$), which included five equally spaced circular delaminations, were prepared for the experiment. Specimens were prepared using either toughened (A specimens) or conventional (B specimens) epoxy resin. Elastic constants for both types of specimens were found to be almost equal, i.e., $E_L = E_T = 41.9$ GPa and $\nu_{LT} = 0.31$ (A specimens) and $E_L = E_T = 41.8$ GPa and $\nu_{LT} = 0.32$ (B specimens), where L and T denote the loading and transverse directions, respectively. Delaminations were introduced into the specimens through placement of two thin ($\approx$0.03 mm thick) Teflon® sheets with delamination size and plate thickness as shown in Table 1. Specimen thickness was chosen to be approximately 2.5 mm following consideration of the test apparatus capacity. The specimens (see Fig. 1) were cut from 300 × 300 mm plates for delaminations to be located at the specimen center. The test region was set to be 150 × 100 mm with the plates clamped at their ends (20-mm width) using steel blocks and then supported 3 mm from both sides by the use of two round edges (Fig. 2) in accordance with a widely used standard experimental technique for measuring

Presented as Paper 94-1368 at the AIAA/ASME/ASCE/AHS/ASC 35th Structures, Structural Dynamics, and Materials Conference, Hilton Head, SC, April 18–20, 1994; received May 20, 1997; revision received March 1, 1998; accepted for publication March 27, 1998.

*Professor, Department of Mechanical Engineering, Faculty of Science and Technology, 7-1 Kioi-cho Chiyodaku. E-mail: suemasu@hoffman.cc.sophia.ac.jp. Member AIAA.

†Graduate Student, Department of Mechanical Engineering, Faculty of Science and Technology, 7-1 Kioi-cho Chiyodaku.

‡Research Associate, Department of Mechanical Engineering, Faculty of Science and Technology, 7-1 Kioi-cho Chiyodaku.

Table 1 Dimensions of tested specimens

Specimen number	Prepreg name	Delamination diameter $2c$, mm	Plate thickness h, mm
A0		——	2.51
A10	F373-30K	10	2.48
A20		20	2.50
A30		30	2.51
B0		——	2.63
B10	F373-06M	10	2.63
B20		20	2.64
B30		30	2.65

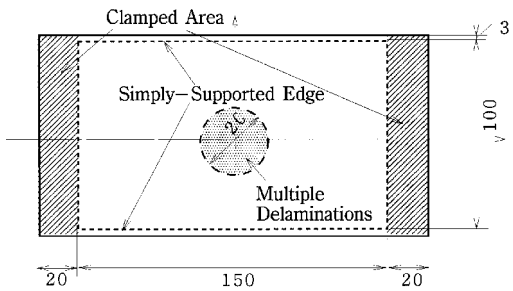

Fig. 1 Schematic of the specimen; all values are given in millimeters.

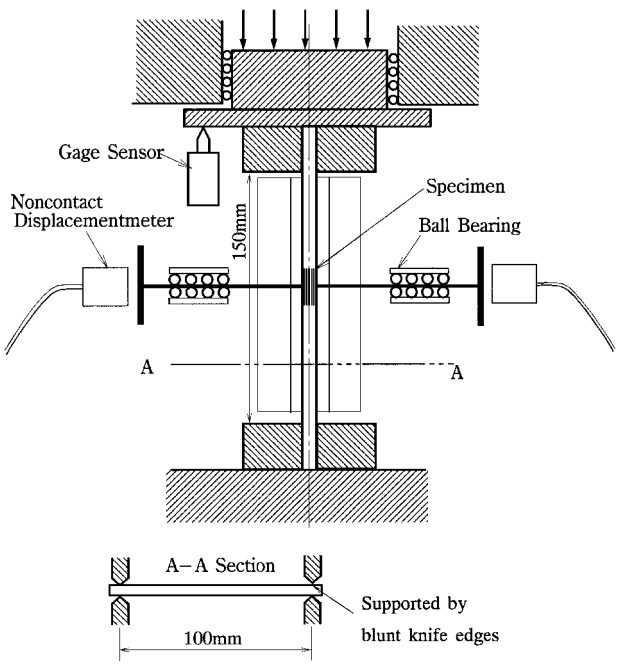

Fig. 2 Schematic of test fixture.

the CAI strength of laminated plates.[22] Solid lubricant (MoS_2) was used along the supported line of the specimen to minimize the friction, whereas a slight gap was necessary between the knife edges and specimen to avoid any large compressive force due to the Poisson effect under loading. This latter procedure was thought to be the main reason for considerable initial imperfection and/or misalignment in the present experiment. Testing of the specimen was undertaken using a cross-head speed of 0.1 mm/min (Shimadzu Autograph 10TB). Transverse deflections were measured with special attention at the center of both front and back specimen surfaces using noncontact displacement meters (Emic NPA-100) because the delaminated portions were thin and, thus, sensitive to any lateral forces. The bars connecting the steel round plates with the specimen were supported by ball bearings to minimize the friction due to the horizontal movement. The test data were stored in a personal computer for further analysis. The experimental setup is shown in Fig. 3.

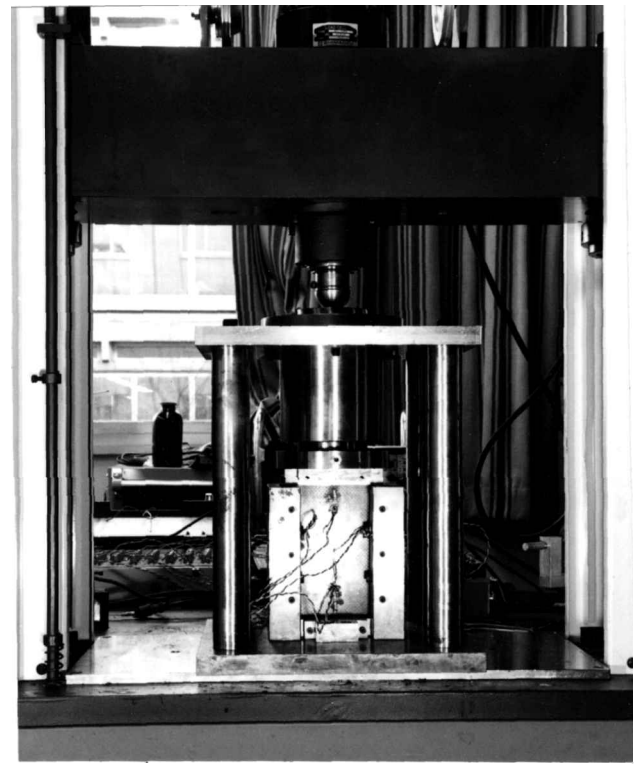

Fig. 3 Photograph of the test setup.

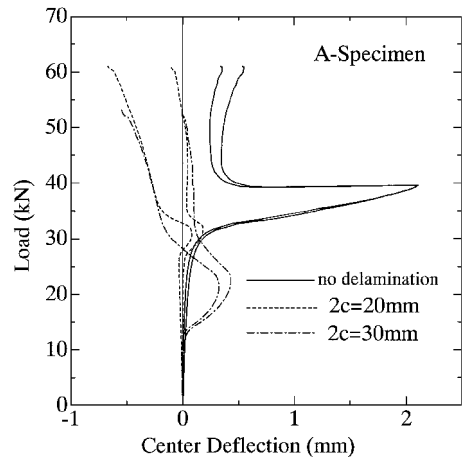

Fig. 4 Compressive load vs center deflection for the specimens.

B. Experimental Results

The relationship between load and center deflections is plotted in Fig. 4. The specimen with no delamination buckled to symmetric shape at approximately 32 kN, showed snap-through behavior from symmetric to antisymmetric at 40 kN, and failed at 62 kN. The buckling load for this specimen was about 10% lower than the theoretical value. Differences between the measured deflections at the front and back surfaces were attributed to the accuracy limit of the displacement meter used and possibly the inclination of the measured points of the plate. Only one of the four undelaminated specimens showed snap-through secondary buckling, whereas the others gradually changed their deformed shape from symmetric to antisymmetric. Because the initial imperfection determines whether snap-through secondary buckling occurs, it may be said that the initial imperfections of the plate were not particularly small. However, this behavior is not critical to the failure process. Not all delaminated specimens that buckled at lower loads, compared to the plate without delaminations, showed unstable snap-through secondary buckling, but instead they gradually changed their deformed shape from symmetric to antisymmetric. The center deflection of the specimen with $2c = 20$ mm grew slightly before it decreased due to an increase

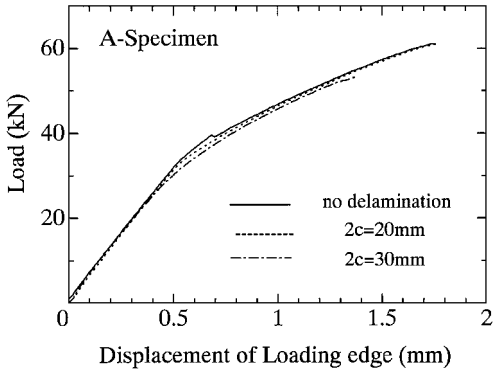

Fig. 5 Compressive load vs end shortening for the specimens.

in the antisymmetric component. The degree of center deflection differed significantly between specimens, as might be expected, because the compressive behavior around the buckling point is known to be sensitive to the initial imperfections and misalignment. The delaminations were believed to open slightly on the antisymmetric postbuckling path. All of the specimens with an antisymmetric shape failed at a load twice as high as the buckling load of the virgin plate.

The relationship between the load and loading edge displacement is presented in Fig. 5. Following buckling, the apparent stiffness of the specimen without delamination was reduced by approximately 30% in the symmetric-dominant deformation region and 60% in the antisymmetric-dominant portion. The curve for $2c = 10$ mm is not plotted in Fig. 5 as it was almost identical to that of $2c = 0$. The stiffness reduction was only slight for the plate with $2c = 30$ mm just following the buckling, which occurred at approximately 13 kN. This is because only the delaminated portion was unstable, whereas the remainder of the plate still possessed significant load-carrying capacity.

Photographs of failed specimens are shown in Figs. 6 and 7, with all cases indicating unstable fracture to have occurred. Specimens without a delamination and those with small delaminations, i.e., A0, A10, A20, B0, and B10, failed at a position approximately one-third of the plate length from the fixed edge, probably due to the bending stress. In the case of specimens with large delaminations, i.e., A30, B20, and B30, the instability of multiple delamination cracks was thought to be the trigger for final failure, with delaminations having spread in the transverse direction.

Buckling and failure loads are plotted against the diameter of the multiple delaminations in Fig. 8. The buckling loads were derived from the relationship between the measured load P and squared deflection δ^2. The buckling load reduction with respect to delamination size was similar for both the A and B specimens. However, failure loads for the B specimens (with conventional epoxy resin) were substantially lower than those of the A specimens (with tougher resin) when the delamination size was large. For example, the failure load for A specimens decreased only 10% for the case of $2c = 30$ mm, whereas the reduction was approximately 30% for the respective B specimens. It was concluded that the buckling load reduction was significant when the diameter of the delaminations exceeded a certain value, which did not depend on the interlaminar toughness of the specimen. However, the strength of the delaminated plate was found to depend on the interlaminar toughness.

III. Analysis

A rectangular transversely isotropic plate fixed along its loading edges and simply supported on its side edges, as shown in Fig. 9, is analyzed following the conditions of the preceding experiments. The plate is assumed to be homogeneous with $N - 1$ circular delaminations of the same radius c and center coordinates (x_0, y_0). The delaminated area is divided into N portions of equal thickness. The classical plate theory is used, and Kirchhoff's hypothesis is assumed even in the neighborhood of the delamination edges. Also, stress concentrations near the crack fronts are not considered. The undelaminated portion is denoted by 0 and the delaminated portions by $I = 1, 2, \ldots, N$.

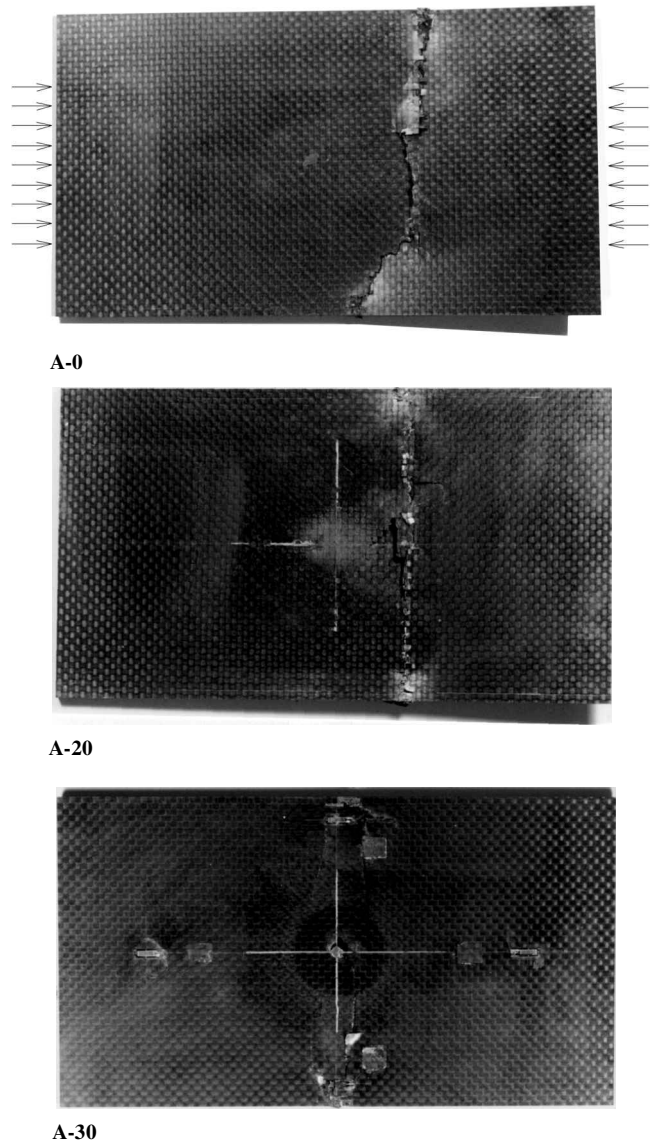

Fig. 6 Photographs of failed specimens with the tougher resin.

Boundary conditions about the out-of-plane displacement w at the loading edges ($x = 0$ and a) and side edges ($y = 0$ and b) are, respectively,

$$w_0 = w_{0,x} = 0, \qquad w_0 = w_{0,yy} = 0 \tag{1}$$

Boundary conditions for the in-plane displacements u and v are given by

$$\begin{aligned} u_0(a, y) - u_0(0, y) &= -a\varepsilon_0 \\ v_0(x, b) - v_0(x, 0) &= \nu_{xy} b\varepsilon_0 \end{aligned} \tag{2}$$

where a and b are the plate length and width, respectively. The value of $a\varepsilon_0$ in Eq. (2) is a prescribed end shortening, whereas values with subscript 0 are the undelaminated region. The parameter ε_0 is an average strain in the x direction when the plate does not deflect, and the inplane shear stress τ_{xy} is assumed to be zero at all of the boundaries. Subscripts following the commas in Eq. (1) denote differentiation with respect to those subscripts. Using Kirchhoff's hypothesis, the continuity conditions about the displacements between the Ith delaminated portion and the undelaminated portion along the circular delamination edge $[(x - x_0)^2 + (y - y_0)^2 = c^2]$ may be simply expressed as

$$w_0 = w_I, \qquad w_{0,n} = w_{I,n} \tag{3}$$

$$u_I = u_0 - z_I w_{,x}, \qquad v_I = v_0 - z_I w_{,y} \tag{4}$$

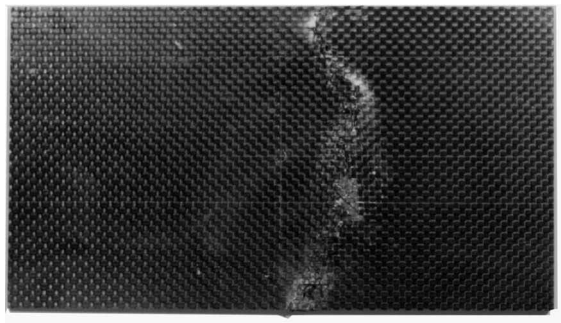

B-0

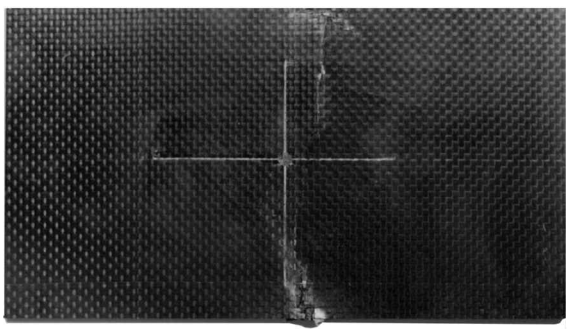

B-20

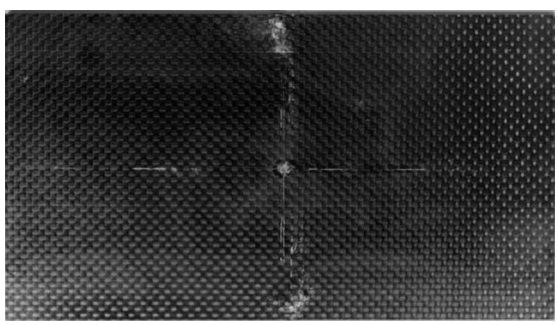

B-30

Fig. 7 Photographs of failed specimens with conventional resin.

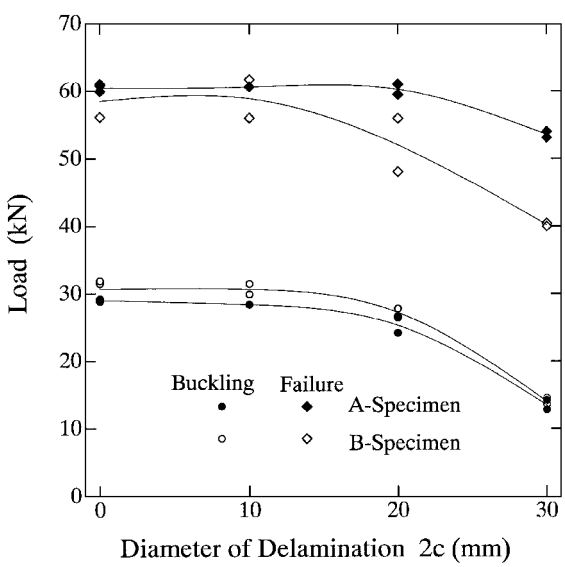

Fig. 8 Effect of delamination diameter on buckling and failure loads for the A and B specimens.

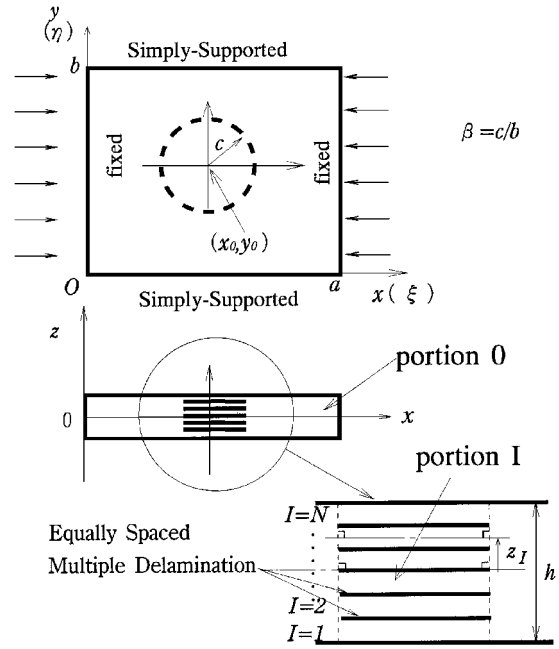

Fig. 9 Analytical model of the specimen.

where the subscript n following the comma denotes differentiation with respect to a coordinate of the outer normal direction of the delamination boundary. Values followed by a subscript I ($I = 1, 2, \ldots, N$) relate to the Ith delaminated portion. In the present analysis, only the case of multiple delaminations located at the plate center is considered, that is, $x_0 = a/2$ and $y_0 = b/2$. Because no load is initially applied to the plate, the potential energy Π is equal to the total strain energy and is expressed as

$$\Pi = \frac{1}{2}\sum_{I=0}^{N}\iint_{S_I}[\{\varepsilon\}^T[A]\{\varepsilon\} + \{\kappa\}^T[D]\{\kappa\}]\,\mathrm{d}x\,\mathrm{d}y \tag{5}$$

where the matrices $[A]$ and $[D]$ are in-plane stiffness and bending stiffness, respectively, for each portion I. As the Rayleigh–Ritz method is applied, kinematically admissible displacement fields should be defined. This may be easily realized by superposing global mode functions, which satisfy the boundary conditions of Eqs. (1) and (2), and local mode functions, which satisfy conditions similar to fixed boundary conditions, that is, displacements u, v, and w in the x, y, and z directions and the slope $w_{,n}$ at the delamination edges are all zero:

$$\begin{aligned} w_0 &= hW_m\phi_m(\xi,\eta) \\ w_I &= h\left[W_m\phi_m(\xi,\eta) + W_m^{(I)}\bar{\phi}_m(\xi,\eta)\right] \end{aligned} \tag{6}$$

$$\begin{aligned} u_0 &= -\varepsilon_0 x + (h^2/a)U_m\,\psi_m(\xi,\eta) \\ u_I &= -\varepsilon_0 x + (h^2/a)\left[U_m\psi_m(\xi,\eta) + U_m^{(I)}\bar{\psi}_m(\xi,\eta) - s_I W_m g_m(\xi,\eta)\right] \end{aligned} \tag{7}$$

$$\begin{aligned} v_0 &= \nu\varepsilon_0 y + (h^2/b)V_m\varphi_m(\xi,\eta) \\ v_I &= \nu\varepsilon_0 y + (h^2/b)\left[V_m\varphi_m(\xi,\eta) + V_m^{(I)}\bar{\varphi}_m(\xi,\eta) - s_I W_m h_m(\xi,\eta)\right] \end{aligned}$$

where W_m, $W_m^{(I)}$, U_m, $U_m^{(I)}$, V_m, and $V_m^{(I)}$ are generalized coordinates to be obtained. The generalized coordinates with superscript (I) are the Ith delaminated portions, whereas functions following the generalized coordinates $\phi_m(\xi,\eta)$, $\bar{\phi}_m(\xi,\eta)$, $\psi_m(\xi,\eta)$, $\bar{\psi}_m(\xi,\eta)$, $\varphi_m(\xi,\eta)$, and $\bar{\varphi}_m(\xi,\eta)$ are the corresponding mode functions. The functions denoted by a bar are the local mode functions, which are zero outside the delaminated portion. The terms $s_I W_m g_m(\xi,\eta)$ and $s_I W_m h_m(\xi,\eta)$ are introduced for in-plane displacement to satisfy continuity conditions along the delamination edges when out-of-plane displacement occurs. The parameter s_I ($= z_I/h$) is the normalized position of each delaminated portion, h is a plate thickness,

and ξ $(=x/a)$ and η $(=y/b)$ are normalized coordinates. A summation convention rule is adopted for convenience. The mode functions are

$$\begin{aligned}
\phi_m(\xi,\eta) &= [\cos\pi(k_m-1)\xi - \cos\pi(k_m+1)\xi]\sin\pi l_m\eta \\
\psi_m(\xi,\eta) &= \sin\pi k_m\xi\cos\pi l_m\eta \\
\varphi_m(\xi,\eta) &= \cos\pi k_m\xi\sin\pi l_m\eta \\
\bar{\phi}_m(\xi,\eta) &= [e(\xi,\eta)]^2 P_{k_m}[(\xi-\xi_0)/\beta]P_{l_m}[(\eta-\eta_0)/\beta] \\
\bar{\psi}_m(\xi,\eta) &= e(\xi,\eta)P_{k_m}[(\xi-\xi_0)/\beta]P_{l_m}[(\eta-\eta_0)/\beta] \\
\bar{\varphi}_m(\xi,\eta) &= e(\xi,\eta)P_{k_m}[(\xi-\xi_0)/\beta]P_{l_m}[(\eta-\eta_0)/\beta]
\end{aligned} \tag{8}$$

where ξ_0 $(=x_0/a)$ and η_0 $(=y_0/b)$ and

$$g_m(\xi,\eta) = \phi_{m,\xi}(\xi_L,\eta)\frac{\xi-\xi_L}{\xi_U-\xi_L} + \phi_{m,\xi}(\xi_U,\eta)\frac{\xi_U-\xi}{\xi_U-\xi_L}$$

$$h_m(\xi,\eta) = \phi_{m,n}(\xi,\eta_L)\frac{\eta-\eta_L}{\eta_U-\eta_L} + \phi_{m,\eta}(\xi,\eta_U)\frac{\eta_U-\eta}{\eta_U-\eta_L}$$

and where

$$P_k(\tau) = \cos[(k\pi/2)(\tau+1)]$$

$$e(\xi,\eta) = \begin{cases} 1-(1/\beta^2)\left[(\xi-\xi_0)^2+(\eta-\eta_0)^2\right] & \text{in the delaminated area} \\ 0 & \text{outside the delaminated area} \end{cases}$$

$$\left.\begin{matrix}\xi_U\\ \xi_L\end{matrix}\right\} = \xi_0 \pm \sqrt{\beta^2-(\eta-\eta_0)^2}$$

$$\left.\begin{matrix}\eta_U\\ \eta_L\end{matrix}\right\} = \eta_0 \pm \sqrt{\beta^2-(\xi-\xi_0)^2}$$

with $\beta = c/b$ the normalized delamination radius. The implicit numbers k_m and l_m are chosen appropriately depending on the type of buckling load to be analyzed. For example, $(k_1, l_1) = (1, 1)$, $(k_2, l_2) = (1, 3)$, $(k_3, l_3) = (3, 1)$, ..., should be selected for the case when symmetric buckling load is requested. As the local mode functions are multiplied by $e(\xi,\eta)$ or $[e(\xi,\eta)]^2$, they satisfy the conditions for local mode functions. Thus, the function P_k has no necessary condition and is satisfactory only if the functions are independent of each other. By substituting Eqs. (6) and (7) into strain–displacement relationships, curvatures and in-plane strains can be expressed with respect to the generalized coordinates as

$$\begin{aligned}
\kappa_{xx}^{(I)} &= -w_{,xx} = -(h/a^2)\left(W_m\phi_{m,\xi\xi} + W_m^{(I)}\bar{\phi}_{m,\xi\xi}\right) \\
\kappa_{yy}^{(I)} &= -w_{,yy} = -(h/b^2)\left(W_m\phi_{m,\eta\eta} + W_m^{(I)}\bar{\phi}_{m,\eta\eta}\right) \\
\kappa_{xy}^{(I)} &= -w_{,xy} = -(h/ab)\left(W_m\phi_{m,\xi\eta} + W_m^{(I)}\bar{\phi}_{m,\xi\eta}\right)
\end{aligned} \tag{9}$$

$$\begin{aligned}
\varepsilon_{x0}^{(I)} &= u_{I,x} + \tfrac{1}{2}w_{I,x}^2 = (h/a)^2\left[-\lambda(a/b)^2 + U_m\psi_{m,\xi} + U_m^{(I)}\bar{\psi}_{m,\xi}\right. \\
&\quad + k_I W_m g_{m,\xi} + \tfrac{1}{2}\left(W_m W_n\phi_{m,\xi}\phi_{n,\xi} + 2W_m W_n^{(I)}\phi_{m,\xi}\bar{\phi}_{n,\xi}\right. \\
&\quad \left.\left. + W_m^{(I)}W_n^{(I)}\bar{\phi}_{m,\xi}\bar{\phi}_{n,\xi}\right)\right] \\
\varepsilon_{y0}^{(I)} &= v_{I,y} + \tfrac{1}{2}w_{I,y}^2 = (h/b)^2\left[\nu\lambda + V_m\varphi_{m,\eta} + V_m^{(I)}\bar{\varphi}_{m,\eta}\right. \\
&\quad + k_I W_m h_{m,\eta} + \tfrac{1}{2}\left(W_m W_n\phi_{m,\eta}\phi_{n,\eta} + 2W_m W_n^{(I)}\phi_{m,\eta}\bar{\phi}_{n,\eta}\right. \\
&\quad \left.\left. + W_m^{(I)}W_n^{(I)}\bar{\phi}_{m,\eta}\bar{\phi}_{n,\eta}\right)\right] \\
\gamma_{xy0}^{(I)} &= u_{I,y} + v_{I,x} + w_{I,x}w_{I,y} \\
&= (h^2/ab)\left[U_m\psi_{m,\eta} + V_m\varphi_{m,\xi} + U_m^I\bar{\psi}_{m,\eta} + V_m^{(I)}\bar{\psi}_{m,\xi}\right. \\
&\quad + k_I W_m\left(g_{m,\eta} + h_{m,\xi}\right) + W_m W_n\phi_{m,\xi}\phi_{n,\eta} + W_m W_n^{(I)}\phi_{m,\xi}\bar{\phi}_{n,\eta} \\
&\quad \left. + W_m^{(I)}W_n\bar{\phi}_{m,\xi}\phi_{n,\eta} + W_m^{(I)}W_n^{(I)}\bar{\phi}_{m,\xi}\bar{\phi}_{n,\xi}\right]
\end{aligned} \tag{10}$$

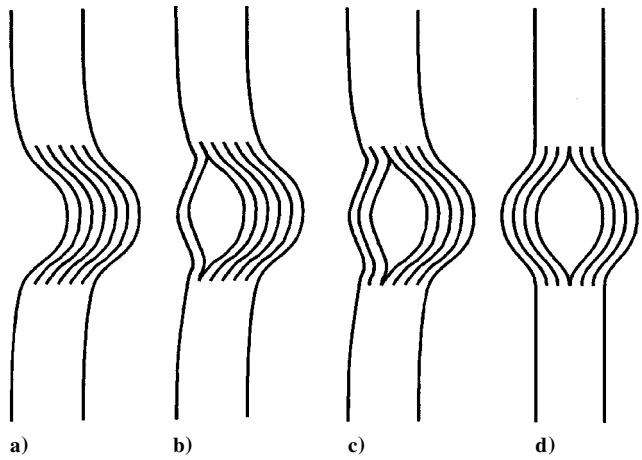

Fig. 10 Schematic of possible buckling modes.

where λ is the nondimensional end shortening and

$$\lambda = (b/h)^2\varepsilon_0$$

Substituting Eqs. (9) and (10) into the potential energy function Π and neglecting higher-order terms, a quadratic expression was obtained for total strain energy with respect to the generalized coordinates:

$$\Pi = A_{ij}q_iq_j + B_{ij}t_it_j + C_{ij}q_it_j + \lambda D_{ij}q_iq_j \tag{11}$$

where the q_i represent the generalized coordinates W_m and $W_m^{(I)}$ and the t_i represent the generalized coordinates U_m, $U_m^{(I)}$, V_m, and $W_m^{(I)}$, respectively. The global in-plane generalized coordinates U_m and V_m need not be considered because they do not couple with the out-of-plane generalized coordinates q_i when only buckling analysis is performed. After differentiating the total potential energy Π by q_i and conducting some manipulations, a standard eigenvalue equation may be obtained, that is,

$$\left[\left(A_{ij} + B_{kl}^{-1}C_{ki}C_{lj}\right) + \lambda D_{ij}\right]q_j = 0 \tag{12}$$

All delaminated portions deform to the same shape, and no delamination opens or overlaps in both the symmetric and antisymmetric buckling modes of the lowest buckling load. When only the lowest buckling load is requested, the delamination opening and contact problem need not be considered. For this case, all of the generalized coordinates relating to the local transverse deflection $W_m^{(I)}$ coincide. The in-plane displacements $U^{(I)}$ and $V^{(I)}$ in the delaminated portions caused by transverse deflection due to buckling are proportional to z_I because the in-plane displacements within the delaminated area are related only to the in-plane displacements along the delamination edges caused by the rotations $w_{,x}$ and $w_{,y}$. Thus, we can impose the following simplified relations on Eqs. (6) and (7) and substantially reduce numerical effort without any increase in the fundamental buckling load:

$$U_m^{(I)} = s_I\bar{U}_m, \qquad V_m^{(I)} = s_I\bar{V}_m, \qquad W_m^{(I)} = \bar{W}_m \qquad (I = 1, 2, \ldots, N) \tag{13}$$

where $\bar{U}_m$, $\bar{V}_m$, and $\bar{W}_m$ are common local coordinates to all of the delaminated portions.

The other buckling deformations shown schematically in Figs. 10b–10d may be realized, depending on initial imperfections, when the buckling load is slightly higher than for the lowest case for the buckling mode in Fig. 10a for large N, on the condition that plate theory is used. The buckling load obtained based on the condition of Eq. (13) is still useful to estimate the load at which the transverse deflection becomes notable because of its simplicity and because no contact condition must be considered.

IV. Results and Discussion

Because deformations observed in the experiment were not only symmetric but also antisymmetric about the line $x = a/2$, both symmetric and antisymmetric buckling behaviors were studied. The mode functions $\phi_{2k-1,2l-1}$ and $\bar{\phi}_{2k-1,2l-1}$ were used for the

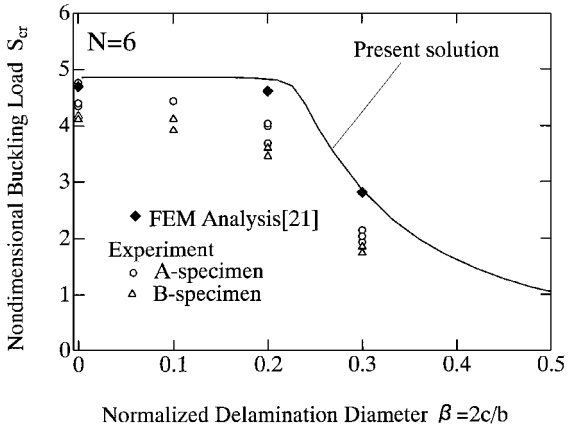

Fig. 11 Comparison of nondimensional buckling loads obtained from experiment and analysis.

symmetric buckling analysis, whereas $\phi_{2k,2l-1}$ and $\bar{\phi}_{2k,2l-1}$ were adopted for the antisymmetric buckling analysis. Convergence of the buckling load with respect to the number of mode functions was quite smooth,[20] with 16 local mode functions ($k \leq 4, l \leq 4$) being sufficient for use in both symmetric and antisymmetric buckling analysis. For symmetric and antisymmetric buckling analysis, 64 ($k \leq 8, l \leq 8$) and 100 ($k \leq 10, l \leq 10$) global mode functions were used, respectively. Both symmetric and antisymmetric buckling modes (of the lowest buckling loads) are physically admissible because of the equal-space assumption of multiple delaminations, as explained in the preceding section, and the contact problem need not be considered. The buckling analysis hereafter is based on the assumption of Eq. (13). If a very accurate value of the buckling load is not necessary, then many of the functions used in the present analysis are not required.

A nondimensional buckling load S_{cr} $\{= P_{cr}/[Ebh(h/b)^2]\}$ is introduced to compare the experimental results with the analytical ones. When the present in-plane boundary condition is studied, this nondimensional buckling load coincides with the normalized end shortening λ_{cr} introduced in the analysis. Nondimensional buckling loads obtained from the experiment and from the present analysis are plotted in Fig. 11 with those from nonlinear finite element analysis.[21] The buckling load can be derived from the postbuckling path of the squared deflection and applied load, which tends to be straight in the case of plate buckling under compression. The accuracy of the buckling load obtained from the present analysis depended on the delamination size, that is, buckling modes observed. The buckling load for undelaminated plate from the present analysis (a typical global dominant-mode buckling) was approximately 3% higher than that from the finite element analysis. When the delamination diameter was large and 0.4 times plate width (a typical local dominant-mode buckling), the difference was very small (only 0.9%). When the diameter was 0.2 times the plate width (strong coupled global–local mode buckling), the error of the present analysis became slightly higher (approximately 5.3%) and the accuracy was slightly poorer. Considering its simplicity and efficiency, the present analysis has some merit. Buckling loads for undelaminated plates obtained from experiments were approximately 10% lower compared to the present analysis, and the case of $2c = 30$ mm was considerably lower than that obtained from the analysis. Differences between results for the undelaminated plates were mainly attributed to the incomplete fixed condition. The low buckling load for the delaminated plate was caused by thinner delaminated layers than expected because total thickness of the inserted Teflon sheets (10×0.03 mm) was more than 10% of the plate thickness, and the delaminated layers seemed to be compressed during fabrication. In the analysis, the symmetric buckling load was always slightly lower compared to the antisymmetric case and was different from the buckling problem of beam plates with multiple delaminations.[8] In the experiment shown in Fig. 4, the center deflection of the front and back surfaces of the delaminated plate first grew in the same direction and then started to decrease. Experimental results that the plate became unstable in the symmetric mode with closed delaminations agree well with the analysis.

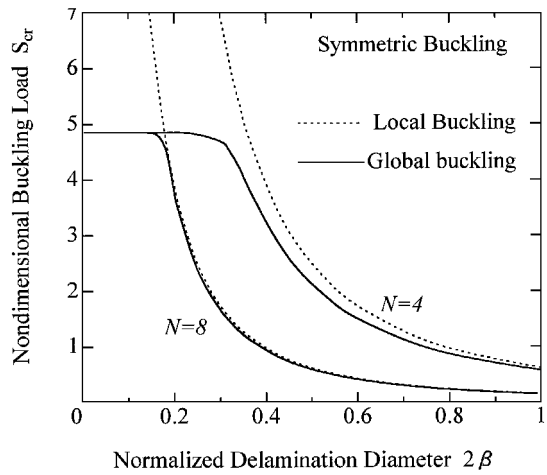

Fig. 12 Comparison of symmetric and antisymmetric buckling loads for global and local modes when $N = 4$ and 8.

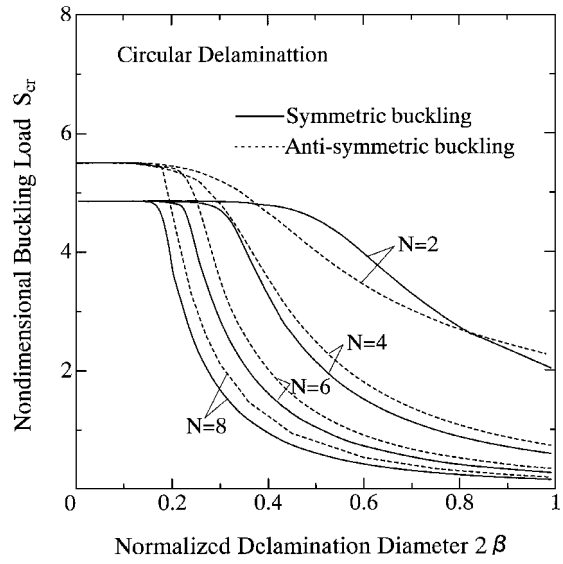

Fig. 13 Nondimensional buckling load vs normalized delamination diameter.

Local buckling and (global) buckling loads are plotted in Fig. 12 for $N = 4$ and 8. The local buckling load was obtained through the use of only local-mode functions. The effect of global deformation on the buckling load, which was fairly significant when N was small, became unimportant when N was large, and the local buckling load was found to be a rough estimate of the reduced buckling load. The local buckling load, which may be easily obtained from the circular plate buckling strain of the delamination size with a fixed boundary, can be used as an approximate estimate of the buckling load for multiply delaminated composite plates due to impact when the number of delaminations is large. This is an important point because the CAI strength for composite laminates subjected to an impact load is significantly reduced compared to the virgin plate and can be roughly estimated from local damage data, such as the size and number of delaminations, without the global plate data, such as the plate size and boundary conditions. However, in reality, the true strength is slightly higher than the buckling load and must be determined precisely by checking whether the energy release rate exceeds the interlaminar toughness of the laminate, or else the maximum stress reaches the laminate strength.

Nondimensional buckling load is plotted against the delamination diameter in Fig. 13. The buckling load is significantly reduced when the delamination size exceeds a certain value, which depends on the number of delaminations. The reduction becomes more significant when the number of delaminations N is large. For example, when $N = 2$, the antisymmetric buckling load is smaller than the symmetric load when $0.2 < \beta < 0.4$, whereas the symmetric buckling load is always smaller compared to the antisymmetric case when $N \geq 4$.

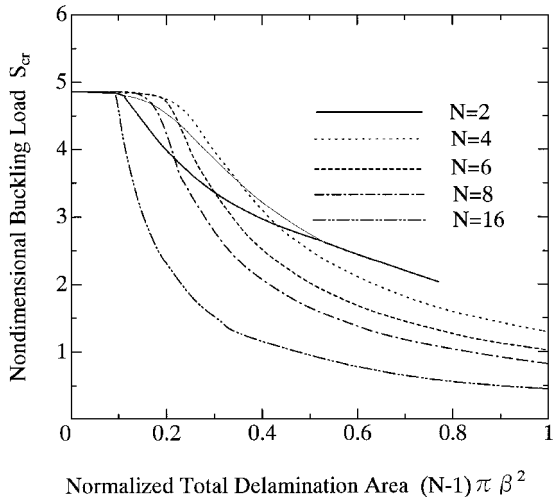

Fig. 14 Nondimensional buckling load vs total delamination area.

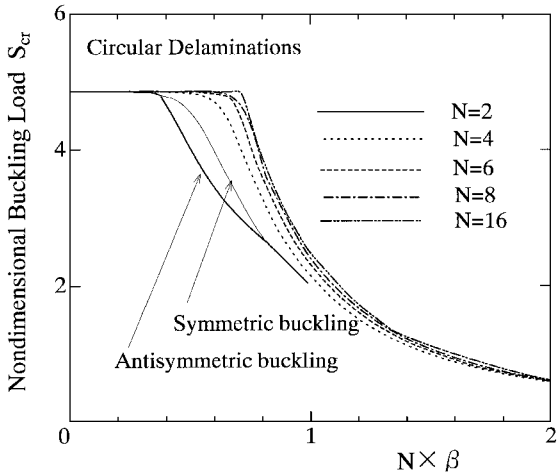

Fig. 15 Nondimensional buckling load vs product of the number of delaminations and delamination radius $N \times \beta$.

The buckling load is plotted against the total area of delamination in Fig. 14. When the total area of delaminations is constant, buckling load reduction is more significant as the number of delaminations increases. Because the total delamination area is known to be approximately proportional to the impact energy, a laminate with more interlaminar surfaces would have a greater reduction in compressive strength. The buckling load is also plotted against $N \times \beta$ in Fig. 15. The parameter $N \times \beta$ can be said to be a governing factor for the buckling load of multiply delaminated plates over which the buckling load starts to reduce, being approximately 0.7 when $N \geq 4$.

V. Conclusions

Results for the present Rayleigh–Ritz analysis agree well with experimental data. From the present experimental and analytical study, the following conclusions may be stated.

1) The compressive strength of a composite plate with multiple delaminations, whose failure is initiated by delamination propagation in the transverse direction, may be significantly improved by the use of a tough resin.

2) Plates with multiple delaminations buckle in a symmetric shape. However, their shape gradually changes with increasing load from symmetric to antisymmetric.

3) The buckling load of a plate decreases with increasing number of multiple delaminations for a given total delamination area. The buckling load is governed not by the total delamination area but by the product of the number of delaminated portions and the delamination radius ($N \times \beta$).

4) Local buckling strain of the circular fixed plate may be used as a first approximation to the buckling load of delaminated plates due to impact as the number of delaminations is usually large.

Acknowledgments

The present research was supported by Ministry of Education, Science and Culture, Japan, Grant Aid for Scientific Research (C) 06650765 and Iketani Science and Technology Foundation Grant 061014-BA. The English was kindly revised by Ian J. Davies, Visiting Scientist of Sophia University.

References

[1]Wang, S. S., Zahlan, N. M., and Suemasu, H., "Compressive Stability of Delaminated Random Short-Fiber Composite, Part I—Modeling and Methods of Analysis," "Part II—Experimental and Analytical Results," *Journal of Composite Materials*, Vol. 19, July 1985, pp. 296–333.

[2]Vizzini, A. J., and Lagace, P. A., "The Buckling of Sublaminate on an Elastic Foundation," *Journal of Composite Materials*, Vol. 21, Dec. 1987, pp. 1106–1117.

[3]Chai, H., and Babcock, C. D., "One Dimensional Modeling of Failure in Laminated Plates by Delamination Buckling," *International Journal of Solids and Structures*, Vol. 17, No. 11, 1981, pp. 1069–1083.

[4]Yin, W. L., "The Effects of Laminated Structure on Delamination Buckling and Growth," *Journal of Composite Materials*, Vol. 22, June 1988, pp. 502–517.

[5]Suemasu, H., "Effects of Multiple Delaminations on Compressive Buckling Behavior of Composite Panels," *Journal of Composite Materials*, Vol. 27, No. 12, 1993, pp. 1172–1192.

[6]Suemasu, H., "Postbuckling Behavior of Composite Panels with Multiple Delaminations," *Journal of Composite Materials*, Vol. 27, No. 11, 1993, pp. 1077–1096.

[7]Chai, H., and Babcock, C. D., "Two Dimensional Modeling of Compressive Failure in Delaminated Laminates," *Journal of Composite Materials*, Vol. 19, Jan. 1985, pp. 67–98.

[8]Yin, W.-L., and Jane, K. C., "Refined Buckling and Postbuckling Analysis of Two-Dimensional Delaminations—I. Analysis and Validation," *International Journal of Solids and Structures*, Vol. 29, No. 5, 1992, pp. 591–610.

[9]Whitcomb, J. D., and Shivakumar, K. N., "Strain-Energy Release Rate Analysis of Plates with Postbuckled Delaminations," *Journal of Composite Materials*, Vol. 23, July 1989, pp. 714–734.

[10]Shahwan, K. W., and Waas, A. A., "A Mechanical Model for the Buckling of Unilaterally Constrained Rectangular Plates," *International Journal of Solids and Structures*, Vol. 31, No. 1, 1994, pp. 23–37.

[11]Suemasu, H., "Compressive Behavior of Fiber Reinforced Composite Plates with a Center Delamination," *Advanced Composite Materials*, Vol. 1, No. 1, 1991, pp. 23–37.

[12]Suemasu, H., "Compressive Behavior of Composite Panels with a Delamination," *Proceedings of Fifth Japan–U.S. Conference on Composite Materials* (Tama-City, Tokyo, Japan), Kokon Shoin, Tokyo, Japan, 1990, pp. 637–644.

[13]Suemasu, H., "Analytical Study of Shear Buckling and Postbuckling Behavior of Composite Plates with a Delamination," *Japan Society of Mechanical Engineers International Journal, Series I*, Vol. 34, No. 2, 1991, pp. 135–142.

[14]Suemasu, H., Gozu, K., Hayashi, K., and Ishikawa, T., "Compressive Buckling of Rectangular Composite Plates with a Free-Edge Delamination," *AIAA Journal*, Vol. 33, No. 2, 1995, pp. 312–319.

[15]Klug, J., Wu, X. X., and Sun, C. T., "Efficient Modeling of Postbuckling Delamination Growth in Composite Laminates Using Plate Elements," *AIAA Journal*, Vol. 34, No. 1, 1996, pp. 178–184.

[16]Ishikawa, T., Sugimoto, S., Matsushima, M., and Hayashi, Y., "Some Experimental Findings in Compression After Impact (CAI) Tests of CF/PEEK(APC-2) and Conventional CF/Epoxy Flat Plates," *Composite Science and Technology*, Vol. 55, No. 4, 1995, pp. 349–363.

[17]Lee, S. M., "Compression-After-Impact of Composites with Toughened Matrices," *SAMPE Journal*, Vol. 22, No. 2, 1986, pp. 64–68.

[18]Prichard, J. C., and Hogg, P. J., "The Role of Impact Damage in Post-Impact Compression Testing," *Composites*, Vol. 21, No. 6, 1990, pp. 503–511.

[19]Dost, E. F., Ilcewicz, W. B., Avery, W. B., and Coxon, B. R., "Effects of Stacking Sequence on Impact Damage Resistance and Strength for Quasi-Isotropic Laminates," *Composite Materials: Fatigue and Fracture*, ASTM STP 1110, American Society for Testing and Materials, 1991, pp. 476–500.

[20]Suemasu, H., "Compressive Behavior of Rectangular Composite Laminates with Multiple Elliptical Delaminations," *Proceedings of Japan–U.S. Conference on Composite Materials* (Kyoto, Japan), Kokon Shoin, Tokyo, 1995, pp. 239–246.

[21]Suemasu, H., and Kumagai, T., "Compressive Behavior of Multiply Delaminated Composite Laminates Part 2: Finite Element Analysis," *AIAA Journal*, Vol. 36, No. 7, 1998, pp. 1286–1290.

[22]SACMA, "Recommended Test Method," Suppliers of Advanced Composite Materials Association, SRM 2-88.

A. M. Waas
Associate Editor